

---

# Vidar: Embodied Video Diffusion Model for Generalist Manipulation

---

**Yao Feng<sup>1†\*</sup>, Hengkai Tan<sup>1\*</sup>, Xinyi Mao<sup>1</sup>, Chendong Xiang<sup>1</sup>, Guodong Liu<sup>1</sup>,  
Shuhe Huang<sup>1</sup>, Hang Su<sup>1</sup>, Jun Zhu<sup>1,2‡</sup>**

<sup>1</sup>Dept. of Comp. Sci. and Tech., Institute for AI, BNRist Center, THBI Lab,  
Tsinghua-Bosch Joint ML Center, Tsinghua University

<sup>2</sup>Shengshu Tech, Beijing, 100084, China  
y-feng23@mails.tsinghua.edu.cn, dcszj@tsinghua.edu.cn

## Abstract

Scaling general-purpose manipulation to new robot embodiments remains challenging: each platform typically needs large, homogeneous demonstrations, and pixel-to-action VLA pipelines typically degenerate under background and viewpoint shifts. In this paper, we present Vidar, a *prior-driven, low-shot adaptation* paradigm that replaces most embodiment-specific data with transferable video priors. Vidar consists of an *embodied video diffusion model* as the generalizable prior and a *masked inverse dynamics model (MIDM)* adapter based on a key decoupling of the policy. The embodied diffusion model is pre-trained on Internet-scale videos and then domain-adapted to 750K multi-view trajectories from three real-world robot platforms using a unified observation space encoding robot, camera, task, and scene contexts. The MIDM module learns action-relevant pixel masks without dense labels, grounding the prior into the target embodiment’s action space while suppressing distractors. Crucially, the generative video prior models the distribution of plausible, temporally coherent interactions, implicitly capturing affordances, contact dynamics, and physical consistency from massive unlabeled video. This shifts the challenge from collecting large amounts of new robot data to efficiently aligning a rich prior with a new embodiment. With only  $\sim$ 20 minutes of human demonstrations on an unseen robot ( $\sim$ 1% of typical data), Vidar outperforms state-of-the-art VLA baselines and generalizes to unseen tasks, backgrounds, and camera layouts. Our results suggest a scalable recipe for “one prior, many embodiments”: strong, inexpensive video priors + minimal on-robot alignment.

## 1 Introduction

Robotic manipulation spans skills such as stable object handling, in-hand reorientation, and multi-point contact control—capabilities underlying cloth folding, liquid pouring, and tool-assisted assembly. Vision-language-action (VLA) models [1, 2, 3, 4] have made encouraging progress via large-scale multimodal pre-training, yet extending them to general-purpose or bimanual settings remains difficult. The core obstacle is control complexity: the action space grows combinatorially with added joints, while success hinges on tight temporal coordination, accurate contact dynamics, and long-horizon reasoning. These factors amplify data requirements and heighten sensitivity to platform-specific details. In practice, progress is constrained by **data scarcity**: human demonstration corpora typically contain only tens to hundreds of hours [5, 3], orders of magnitude smaller than Internet-scale video collections with hundreds of thousands of hours [6]. Collecting demonstrations is labor-intensive, expensive, and coupled to hardware, leaving a key question: *how can a new robot embodiment achieve precise, generalizable control with limited domain-specific data?*

---

\*Equal contribution; †Part of the work was done during intern at Shengshu; ‡The corresponding author.

A natural answer lies in *video*. Unlike text or static images, video is both abundant and intrinsically suited to capture the temporal dynamics and interaction cues—affordances, contacts, motion continuity—that demonstrations aim to convey. Leveraging such signals enables robots to acquire embodiment-agnostic interaction knowledge at scale, and later specialize to new morphologies with far fewer platform-specific samples. To turn this rich modality into a transferable prior, we adopt video generative models, which learn distributions of *plausible, temporally coherent rollouts* rather than task-specific labels. This generative formulation enforces physical consistency, supports counterfactual reasoning about “what could happen next”, and shifts dependence from costly demonstrations to abundant raw video. Recent advances in video diffusion models trained on web-scale corpora already show strong semantic grounding and temporal fidelity [7, 8, 9, 10], making them well-suited to serve as general interaction priors for low-shot embodiment alignment. Meanwhile, for robot control, our objective departs from vanilla video diffusion. Rather than producing photorealistic clips, we require *actionable* rollouts that are consistent with robot actuation, accurate in contact dynamics, and robust across embodiments.

In this paper, we propose **Video Diffusion for Action Reasoning (Vidar)**, the first effort to fully explore the strong prior learned from Internet-scale videos for efficient bimanual manipulation with decoupled *video generation* and *action prediction*. To build a good video prior for embodied control, we propose a three-stage training pipeline, where Internet-scale videos are used for general pre-training, large cross-embodiment robotic datasets are used for embodied domain pre-training, and a small number of robot-specific demonstrations are used for target domain fine-tuning. Specifically for embodied domain pre-training, we align 750K multi-view bimanual clips spanning three robot platforms into a unified observation space. Such pre-training on a unified space ensures control feasibility, promotes physically credible contacts, and mitigates viewpoint and morphology gaps. During inference, we further enhance rollout quality by applying test-time scaling [11] together with physics-aware reranking, improving temporal coherence and fidelity.

On the action side, the main challenge is to decode videos into reliable controls despite background clutter, distractors, and partial observability of hands and tools. We address this with a **Masked Inverse Dynamics Model (MIDM)**, which learns to attend selectively to action-relevant regions without pixel-level supervision. By filtering out irrelevant content, MIDM provides robust action decoding and facilitates the transfer of video priors across domains. Moreover, such a lightweight model can be trained using only a small number of demonstrations. Together, these components transform raw Internet video into a transferable and controllable prior, enabling precise manipulation with only a small number of demonstrations.

Empirically, Vidar achieves state-of-the-art performance on the RoboTwin [12] benchmark, while only using 40% of the training data. In the real world, it attains strong performance with only **20 minutes of human demonstrations** (roughly 3 per task) on a previously unseen robotic platform. Despite this minimal supervision, it outperforms leading baselines by large margins—**58%** over VPP [13] and **40%** over UniPi [14]. Moreover, it generalizes robustly to novel scenarios, such as environments with reflective surfaces, indicating that video-pretrained priors can support both data-efficient adaptation and semantically grounded control.

## 2 Method

In this section, we formally define our problem and present Vidar in detail. The overview of our method is shown in Figure 1.

### 2.1 Problem Formulation

This work investigates the challenges of bimanual manipulation for everyday activities, tasks that are inherently resistant to standardization. Our experiments are conducted using the common Aloha robot platform [3, 15], with detailed hardware specifications given in Appendix F. The problem is formulated as follows.

Let  $\mathcal{L}$  denote the language instruction space,  $\mathcal{O}$  the observation space, and  $\mathcal{A}$  the action space. Our goal is to learn a conditional manipulation policy

$$\pi : \mathcal{L} \times \mathcal{O} \rightarrow \mathbb{P}(\mathcal{A}),$$

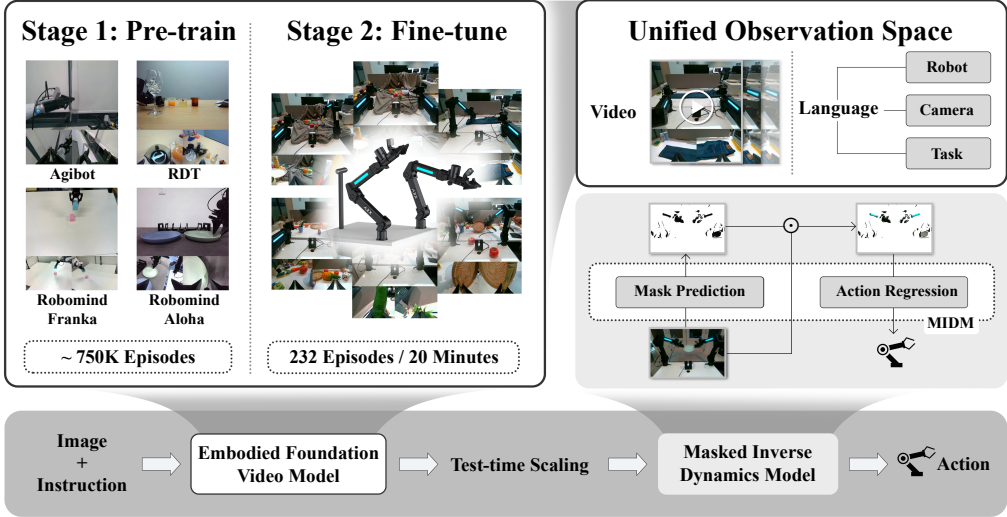


Figure 1: The overall pipeline of Vidar, where various video sources are leveraged for transferring to a new platform with limited demonstrations. A unified observation space handles heterogeneous, multi-view robotic videos and language instructions, enabling the pre-training of an embodied foundation video model on about 750,000 multi-view bimanual robotic episodes. After fine-tuning it with only 20 minutes of human demonstrations on an unseen robot platform, we adopt test-time scaling to select the best video during inference. Meanwhile, the masked inverse dynamics model (MIDM) converts videos to actions, where masks are learned to attend to action-relevant regions for background-robust action regression.

where  $\mathbb{P}(\cdot)$  denotes probability measures over the corresponding space. Learning this policy directly is highly challenging. It requires large-scale demonstrations that jointly cover language, observation, and action, which are expensive and hardware-specific. Moreover, robots differ in sensing, morphology, and viewpoints, making policies learned on one platform difficult to transfer. Finally, successful manipulation depends on fine-grained contact events and long-horizon temporal coherence; photorealistic video generation alone does not guarantee *actionability*.

We address these challenges by elevating the action space to the video domain, where richer semantic information is preserved and an abundance of large-scale data is available for learning a strong, transferable prior. We factorize the policy through the video space  $\mathcal{V}$ :

$$\pi = I \circ G, \quad G : \mathcal{L} \times \mathcal{O} \rightarrow \mathbb{P}(\mathcal{V}), \quad I : \mathcal{V} \rightarrow \mathcal{A}.$$

Here,  $G$  is a video generation model that produces temporally coherent, physically plausible rollouts conditioned on task and observations, while  $I$  is an inverse dynamics model that maps short video windows into robot-specific controls. This two-stage design shifts most of the representation burden to  $G$ , which can be pretrained on abundant Internet and robotic video, and leaves only a lightweight  $I$  to be trained with limited demonstrations on the target platform.

Concretely,  $G$  is conditioned on proprioceptive traces and embodiment tokens, and trained on 750K multi-view bimanual clips from three robot platforms, aligned into a unified observation space. This ensures that generated rollouts remain feasible under different morphologies and camera setups, and that contact and motion continuity are preserved. At inference, test-time scaling [11] with physics-aware reranking further improves temporal coherence and physical plausibility. The inverse dynamics component  $I$  is instantiated as a **Masked Inverse Dynamics Model (MIDM)**, which learns to attend to action-relevant regions such as hands, tools, and contact patches without pixel-level labels. By filtering out background clutter and distractors, MIDM provides robust action decoding and enables effective transfer of video priors across domains.

This formulation directly addresses the identified challenges: large-scale video pretraining reduces the need for triply-labeled demonstrations; conditioning and unified observation mitigate embodiment shifts; contact- and flow-consistent objectives make rollouts actionable; and MIDM grounds them

to the target robot with few demonstrations. Together, these design choices turn raw video into transferable interaction priors that enable efficient and precise adaptation to new robotic embodiments.

## 2.2 Video Generation Model

We adopt rectified flow [16, 17] models, which generate high-quality videos by modeling pixel flow over time. Specifically, the model parameterizes a flow function  $v : \mathcal{V} \times \mathbb{R} \times \mathcal{L} \rightarrow \mathcal{V}$ , which models the velocity of pixels as they transition from noisy video frames to target frames under certain conditions and time, leading to the following ODE over a video  $x_t$  (with  $x_0$  sampled from a Gaussian and  $x_1$  as the output video):

$$\frac{dx_t}{dt} = v(x_t, t, c), \quad t \in [0, 1]. \quad (1)$$

To learn the non-trivial mapping between the Gaussian distribution and the video distribution, we train the “velocity”  $v$  to approximate the constant flow from  $x_0$  to  $x_1$  during training. The flow matching loss is:

$$L_G = \mathbb{E}_{c, t, x_0, x_1} \left[ \|(x_1 - x_0) - v(tx_1 + (1-t)x_0, t, c)\|^2 \right]. \quad (2)$$

**Unified Observation Space.** To mitigate viewpoint and morphology gaps between heterogeneous embodiments, we design a unified observation space for multi-view embodied data. Denoting the number of cameras as  $V$ , we can define a unified observation space  $\mathcal{U} \subseteq \mathcal{L} \times \mathcal{O}$  (also see Figure 1):

$$\mathcal{U} = \{\langle \mathbf{o}, \mathbf{l} \rangle | \mathbf{o} = \text{aggregate}(\mathbf{I}^{(1)}, \mathbf{I}^{(2)}, \dots, \mathbf{I}^{(V)}), \mathbf{l} = \text{concatenate}(l_r, l_c, l_t)\}, \quad (3)$$

where  $\text{aggregate}(\mathbf{I}^{(1)}, \mathbf{I}^{(2)}, \dots, \mathbf{I}^{(V)})$  is the aggregation of multi-view images, and  $l_r$ ,  $l_c$ , and  $l_t$  are instructions related to the robotic platform, camera, and task, respectively. Specifically, each observation  $\mathbf{o}$  is constructed as  $\mathbf{o} = \bigoplus_{k=1}^V \phi_{r_k}(\mathbf{I}^{(k)})$ , where  $\mathbf{I}^{(k)}$  is the RGB image from camera  $k$ ,  $\phi_{r_k}$  is a spatial resizing function. This operation produces a consistent tensor shape across platforms and preserves both semantic and kinematic context. Instead of relying solely on task information and a single view, we condition the video generation model on the robot, camera, task information, and multiple views, thereby providing rich context for video prediction with unified representations across heterogeneous embodiments.

**Embodied Pre-training and Fine-tuning on Unified Observation Space.** We pre-train our video generation model on a large-scale corpus of approximately 750K open-sourced episodes, all projected into the unified observation space (Equation (3)). This dataset includes three camera views, a configuration commonly adopted in bimanual setups [15, 18] to provide abundant context information for precise control. At fine-tuning time, we apply supervised fine-tuning (SFT) on all model parameters using a small number of human demonstration episodes collected from the target platform. To ensure precise adaptation without overfitting, we augment the dataset by clipping variable-length videos from random starting points. In this way, the limited domain-specific data is fully used, and the model learns to predict videos at various states.

**Test-time Scaling.** Diffusion-based video generation is inherently stochastic, resulting in significant variance in the quality, physical plausibility, and task relevance of sampled rollouts. Naively sampling a single trajectory may result in incoherent or suboptimal generations, especially in cluttered or ambiguous scenes. To address this, we propose a test-time scaling strategy: given an observation prefix  $\mathbf{o}_1$ , we generate  $K$  candidate video trajectories  $\{\tilde{\mathbf{v}}_{1:T}^{(i)}\}_{i=1}^K$  using different random seeds. We then rank these trajectories using a pretrained evaluator (e.g., CLIP or a vision-language model)  $q_\eta$  and select the highest-scoring one, i.e.,  $\arg \max_i q_\eta(\tilde{\mathbf{v}}_{1:T}^{(i)})$ . This approach aligns the predicted video distribution with task-relevant, actionable videos through “rejection sampling”, reducing sampling variance and consistently improving the quality of generated demonstrations..

## 2.3 Masked Inverse Dynamics Model

Inverse dynamics models often suffer from poor generalization due to the presence of background noise, texture biases, and visual distractions in high-dimensional observations [19]. Explicitly localizing action-relevant regions is challenging without dense annotations, and existing segmentation

methods [20] often fail to capture both arms in the bimanual settings, let alone produce temporally consistent segmentations (see Figure 6 in Appendix C).

To solve the problem, we introduce a masked inverse dynamics model (MIDM) that learns to focus on task-relevant regions via implicit mask prediction. The model consists of two components: (1) a mask prediction network  $U$  that outputs a spatial mask  $m \in [0, 1]^{H \times W}$  from an input frame  $x$ , and (2) an action regression network  $R$  that predicts the action from the masked frame. Formally:

$$m = U(x), \quad \hat{a} = R(\text{Round}(m) \odot x),$$

where  $\odot$  denotes element-wise multiplication, and  $\text{Round}(\cdot)$  means rounding to the nearest integer. The model is trained by minimizing the following loss:

$$L_I = \mathbb{E}_{x,a} [l(\hat{a} - a) + \lambda \|m\|_1],$$

where  $l(\cdot)$  is the Huber loss. The second  $\ell_1$ -norm regularization term promotes spatial sparsity, encouraging the model to focus on minimal, task-critical regions without any segmentation supervision. We train it using straight-through estimators. By utilizing reliable action signals as supervision, rather than noisy annotations, our method demonstrates robust generalization to unseen environments and backgrounds, as evidenced by our experimental results (Section 3).

### 3 Experiments

We now present experimental studies, with the goal to verify the following hypotheses:

- H1:** Vidar achieves superior success rates with only 20 minutes of target domain demonstrations;
- H2:** Vidar generalizes effectively to unseen tasks and backgrounds;
- H3:** Pre-training with a unified observation space benefits embodied video generation;
- H4:** Masked inverse dynamics models exhibit greater generalization ability than the baseline.

#### 3.1 Experimental Setup

##### 3.1.1 Datasets

For pre-training, we utilize episodes sourced from Agibot-World [18], RoboMind [21], and RDT [3]. As is required by the unified observation space, we provide descriptions of the robot type and camera placements in addition to the provided task instructions. The resulting pre-training dataset for real-world experiments comprises 746,533 episodes. For the simulation experiments, we additionally add episodes from Egodex [22].

For the simulation domain, we collect 20 episodes per task on the Aloha (agilex) robot under clean scenarios of the RoboTwin platform [12], which is 40% of the data usage of their leaderboard. For the real-world target domain, we collect 20 minutes of human demonstration videos, covering 81 tasks across 232 episodes. This dataset is used to both fine-tune the video diffusion model and to train the masked inverse dynamics model. For more details of our datasets, see Appendix A.

##### 3.1.2 Training and Inference

We evaluate our method using two representative video generation models: the open-source Wan2.2 [8] for simulation experiments, and Vidu 2.0 [10] for the more diverse and challenging real-world tests. We train the models with a batch size of 128, where the first 10,000 steps involve pre-training on the diverse robotics dataset, followed by 12,000 fine-tuning steps for Wan2.2 and 13,000 fine-tuning steps for Vidu 2.0. To reduce inference costs, we uniformly downsample the training videos to 8 frames per second (fps). For the masked inverse dynamics model, we adopt the U-Net [23] structure as the mask prediction network and the ResNet [24] structure as the action regression network, with  $\lambda = 3 \times 10^{-3}$  (effects of  $\lambda$  are shown in Appendix C). We train it exclusively on the fine-tuning dataset. We use AdamW [25] for all our training. Here are some detailed settings of real-world experiments.

We use open-loop control for Vidar; the videos are generated in a single batch, without subsequent generation after the initial run. Using 8 NVIDIA Ampere-series 80GB GPUs, generating one video with 60 frames (7.5 seconds duration at 8fps) costs about 25 seconds. The time cost can be reduced

using distillation or quantization, which are beyond the scope of this paper. For test-time scaling, we choose  $K = 3$ , and three videos with different random seeds are generated in parallel, evaluated by GPT-4o [26]. More details of training and inference can be found in Appendix B.

To demonstrate the generality of our approach, we also reproduce real-world experiments using the open-sourced HunyuanVideo model [9]. Related results are shown in Appendix E.

### 3.1.3 Baselines

For simulation experiments, there are a lot of methods on the RoboTwin leaderboard. For real-world experiments, we perform preliminary experiments over multiple baselines and find that adaptation with only 20 minutes of videos and about 3 demonstrations per task is too challenging for vision-language-action models. Thus, we choose two baselines that also incorporate video-level prior knowledge: UniPi and VPP. To ensure fair comparison, we reproduce these methods over the advanced Vidu 2.0 model.

**UniPi.** We fine-tune the Vidu 2.0 model directly on our demonstration data, without any additional pre-training on our large robotics dataset. Additionally, we train an inverse dynamics model using a ResNet architecture.

**VPP.** We use the same checkpoint for the video generation model as our method, and train a diffusion model to generate short action sequences based on the latent features during one-step video generation and CLIP [27] embeddings of the task instructions. Notably, they use closed-loop control, which means new action sequences are generated and executed after previous executions.

## 3.2 Experimental Results

**H1: Success Rates.** For simulation experiments, we evaluate our method on the RoboTwin 2.0 [12] benchmark. Trained with only 20 episodes per task from clean scenarios, our method achieves an average success rate of 60.0% in clean scenarios and 14.5% in randomized scenarios across 50 tasks. With only 40% data usage relative to the leaderboard, we achieve a state-of-the-art average success rate in clean scenarios, surpassing strong baselines like Pi0 [28]. Detailed results are provided in Appendix C. For real-world experiments, we test two baseline methods and our method under three scenarios: seen task and background (six tasks), unseen task (five tasks), and unseen background (six tasks). Detailed explanations are as follows:

- **Seen Tasks & Backgrounds:** three pick-and-place tasks (e.g., grasp tomato using left arm), two daily-life tasks (e.g., flip dice using right arm), and one bimanual task (lift the basket). The background we use is a cluttered office desk setup, featuring several computers situated behind the workspace.
- **Unseen Tasks:** three daily-life tasks (e.g., stack the bowl on the steamer using the left arm) and two semantic tasks (e.g., grasp the shortest bread using the left arm).
- **Unseen Backgrounds:** two pick-and-place tasks (e.g., grasp a tomato using the left arm) and four daily-life tasks (e.g., flip a dice using the left arm). For unseen backgrounds, we include a studio setup with a typical green screen and a daily workspace setting with two cupboards containing robot supplies, which exhibit reflective surfaces.

The success rates are shown in Table 1. We find that our method achieves superior success rates over all three scenarios, demonstrating the effectiveness of our method. UniPi does not utilize heterogeneous robotic data, which restricts its generalization under limited demonstrations; VPP uses predicted features from a single denoising forward pass for action prediction, which leads to noise and instability—particularly in unseen environments. More details can be found in Appendix C.

**H2: Generalization Ability.** For the simulation benchmark, we show that our model generalizes effectively to randomized scenarios, despite being trained only on clean scenarios (see Appendix C). For real-world experiments, quantitative results of our superior generation ability are shown in unseen scenarios of Table 1. We also provide some demonstrations in Figure 2, where Vidar demonstrates robust generalization to unseen tasks and backgrounds with strong semantic understanding. In Appendix D, we present more visualizations, including failure cases.

Table 1: Success rates of different methods and configurations over robot manipulation tasks. Vidar achieves high success rates across all three scenarios, with great generalization ability to unseen tasks and backgrounds.

Method	Seen Tasks & Backgrounds	Unseen Tasks	Unseen Backgrounds
VPP	4.5%	13.3%	0.0%
UniPi	36.4%	6.7%	22.2%
<b>Vidar (Ours)</b>	<b>68.2%</b>	<b>66.7%</b>	<b>55.6%</b>

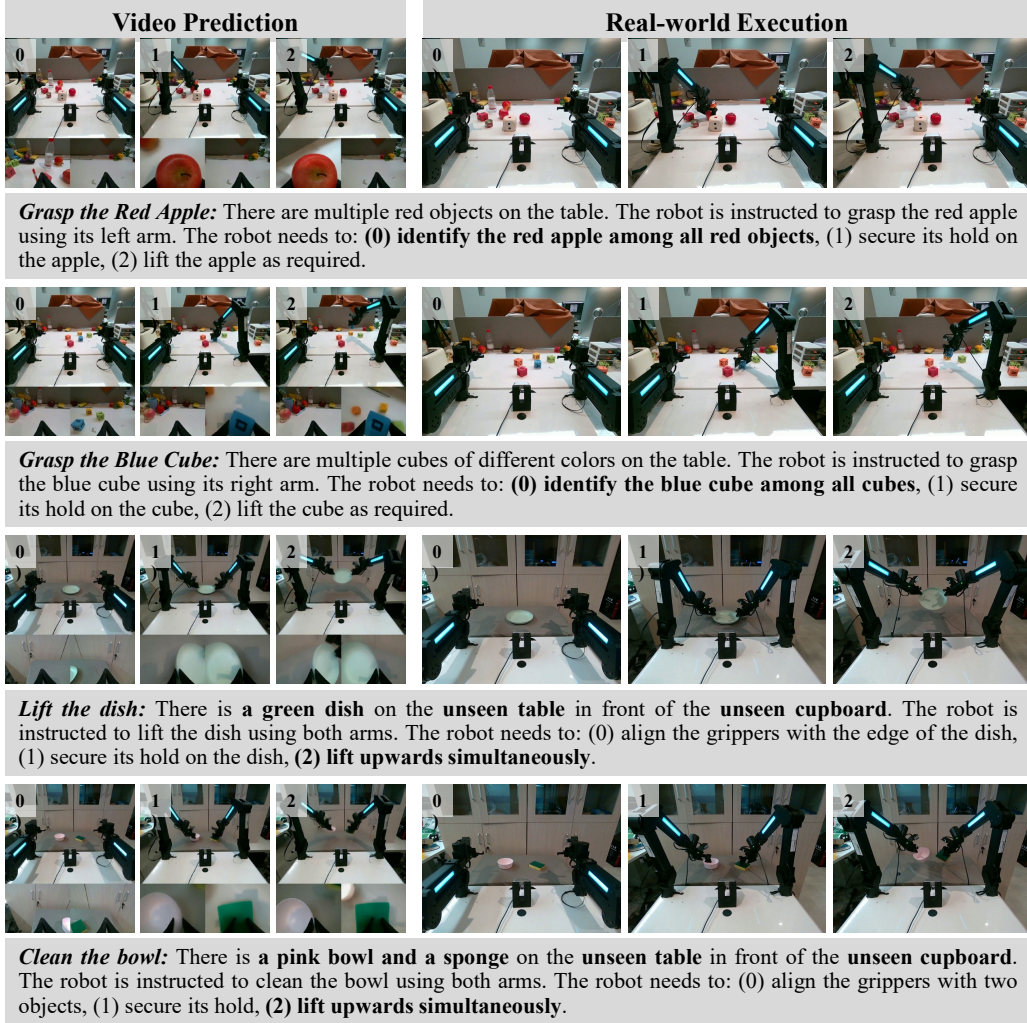


Figure 2: Videos of predictions (left) and corresponding executions (right) of Vidar for challenging tasks. It can handle unseen tasks and unseen backgrounds with strong semantic understanding.

**H3: Effectiveness of Pre-training.** We evaluate the video generation quality of the original Vidu 2.0 model and our pre-trained version over the unseen target domain using VBench [29]. As is shown in Table 2, we find that pre-training using large-scale robotic videos under our unified observation space enhances both the consistency and quality of generated frames, which are important for robot control tasks.

**H4: Effectiveness of MIDM.** Based on empirical observations of the Aloha robot’s error tolerances, we define a successful prediction as having a maximum infinity norm error of less than 0.06 for joint positions and less than 0.6 for gripper positions, for both arms. Using this criterion, we evaluate the

Table 2: VBench video quality measurements for different video model configurations in the unseen target domain. Embodied pre-training over the unified observation space benefits video generation.

Configuration	Subject Consistency	Background Consistency	Imaging Quality
Vidu 2.0	0.565	0.800	0.345
<b>+ Embodied Pre-training</b>	<b>0.855</b>	<b>0.909</b>	<b>0.667</b>

success rates of our masked inverse dynamics model (MIDM) and a ResNet baseline on both training and testing sets. The results, presented in Table 3, show that our MIDM demonstrates superior generalization compared to the baseline. Additionally, examples of the learned masks are provided in Figure 3. Without any additional supervision, MIDM effectively captures action-relevant features and generalizes well to unseen backgrounds.

Table 3: Training and testing success rates and testing  $l_1$  errors of different inverse dynamics models. Both the baseline and MIDM achieve high performances during training, but MIDM generalizes better during test time.

Inverse Dynamics Model	Training Accuracy	Testing Accuracy	Testing $l_1$ Error
ResNet	<b>99.9%</b>	24.3%	0.0430
<b>MIDM (Ours)</b>	<b>99.9%</b>	<b>49.0%</b>	<b>0.0308</b>



Figure 3: Input images and corresponding masked images learned by the masked inverse dynamic model (MIDM). The two cases are from an unseen background with complex reflective surfaces, while the predicted mask images still focus on the essential parts of robotic arms.

### 3.3 Ablation Study

We conduct an ablation study of our method by evaluating success rates on the same tasks presented in Table 1. The results are summarized in Table 4, where “w/o MIDM” means using the ResNet baseline. We find that both masked inverse dynamics models and test-time scaling are beneficial to the success rates.

## 4 Related Work

**Vision-Language-Action Models (VLAs).** Vision-Language-Action (VLA) models integrate perception, language understanding, and action generation to enable general-purpose embodied intelligence. However, existing VLA systems rely heavily on large-scale, task-specific datasets—often requiring hundreds of thousands of trajectories—to achieve robust performance. For instance, RT-1 [30] uses 130K real-world episodes, while RT-2 [31] scales to 1B image-text pairs. Recent works like OpenVLA [2], Octo [32], Pi0 [28], and RDT-1B [3] further expand to millions of demonstrations across diverse embodiments. Despite these efforts, such data-intensive pipelines present a scalability bottleneck and limit generalization to novel tasks and domains, motivating more data-efficient and transferable alternatives.

**Video Generation Models for Embodied AI.** Video generation models for embodied AI predict future scene dynamics to assist robotic planning and policy learning. Current works such as UniPi [14],

Table 4: Ablation study of Vidar, where “w/o MIDM” means using the ResNet baseline. In three scenarios, both masked inverse dynamics models and test-time scaling are beneficial to the success rates.

Configuration	Seen Tasks & Backgrounds	Unseen Tasks	Unseen Backgrounds
Vidar w/o TTS	45.5%	33.3%	44.4%
Vidar w/o MIDM	59.1%	26.7%	22.2%
<b>Vidar (Ours)</b>	<b>68.2%</b>	<b>66.7%</b>	<b>55.6%</b>

RoboDreamer [33], Gen2Act [34], CLOVER [35], SuSIE [36], and GR-1 [37] mainly adopt text-conditioned video generation or frame prediction with a fixed single-camera view, demonstrating how a single-arm robot physically compliantly executes a series of actions. Additionally, Genie 2 [38] generates interactive 3D environments via autoregressive latent diffusion, enabling scalable training for embodied agents. These models implicitly encode physical laws through video synthesis, reducing reliance on real-world robotics data. However, current works mostly remain limited to single-arm robots and rely on a single camera view, which restricts their applicability in more complex real-world scenarios; meanwhile, the success of Instant3D [39] provides a compelling demonstration that the diffusion models can effectively adapt to multi-view formats. Moreover, most existing methods do not utilize heterogeneous embodied videos for pre-training.

**Coupled Video Generation and Action Synthesis.** Recent efforts couple video generation with action synthesis to enhance physical consistency and interoperability. For instance, Video-Prediction-Policy (VPP) [13] learns implicit inverse dynamics conditioned on future representations predicted by a video diffusion model, while UVA [40] unifies video-action latent spaces with lightweight diffusion heads. Other works, such as VidMan [41] and Dreamitate [42], integrate low-level action representations with video prediction to predict actions. These approaches bridge spatiotemporal dynamics between vision and action, offering novel solutions for complex manipulation tasks. However, these approaches require end-to-end joint training of video generation and action prediction models, which limits their flexibility and adaptability.

## 5 Conclusion

We presented Vidar, a generalizable framework for bimanual robotic manipulation that addresses the core challenges of data scarcity and embodiment heterogeneity. By combining large-scale, diffusion-based video pretraining over a unified observation space with a masked inverse dynamics model, Vidar enables accurate action prediction from multi-view visual observations and language instructions, requiring only minimal demonstrations in new environments. Our experiments demonstrate that Vidar consistently outperforms existing methods and exhibits strong generalization to unseen tasks and backgrounds, highlighting its capacity for semantic understanding and transfer.

## 6 Ethics Statement

Vidar has the potential to accelerate the deployment of capable bimanual robots in real-world environments. However, the rise of generalist robotic systems also introduces important considerations regarding privacy, safety, and accountability, especially as these systems are deployed in sensitive domains involving close human-robot interaction.

## 7 Reproducibility Statement

We submit our code, including the HunyuanVideo diffusion model and the masked inverse dynamics model, in the supplemental materials. Meanwhile, the Wan2.2 model that we use is open-sourced and widely available. Appendix A describes our dataset in detail, and Appendix B provides comprehensive information on training and inference. All datasets used for pre-training are publicly available.

## References

- [1] Abby O'Neill et al. "Open X-Embodiment: Robotic Learning Datasets and RT-X Models : Open X-Embodiment Collaboration". In: *IEEE International Conference on Robotics and Automation, ICRA 2024, Yokohama, Japan, May 13-17, 2024*. IEEE, 2024, pp. 6892–6903.
- [2] Moo Jin Kim et al. "OpenVLA: An Open-Source Vision-Language-Action Model". In: *Conference on Robot Learning, 6-9 November 2024, Munich, Germany*. Ed. by Pulkit Agrawal, Oliver Kroemer, and Wolfram Burgard. Vol. 270. Proceedings of Machine Learning Research. PMLR, 2024, pp. 2679–2713.
- [3] Songming Liu et al. "RDT-1B: a Diffusion Foundation Model for Bimanual Manipulation". In: *CoRR* abs/2410.07864 (2024).
- [4] Yunhao Zhang and Junchi Yan. "Crossformer: Transformer Utilizing Cross-Dimension Dependency for Multivariate Time Series Forecasting". In: *The Eleventh International Conference on Learning Representations, ICLR 2023, Kigali, Rwanda, May 1-5, 2023*. OpenReview.net, 2023.
- [5] Physical Intelligence et al. " $\pi_{0.5}$ : a Vision-Language-Action Model with Open-World Generalization". In: *CoRR* abs/2504.16054 (2025).
- [6] Yi Wang et al. "InternVid: A Large-scale Video-Text Dataset for Multimodal Understanding and Generation". In: *The Twelfth International Conference on Learning Representations, ICLR 2024, Vienna, Austria, May 7-11, 2024*. OpenReview.net, 2024.
- [7] Yixin Liu et al. "Sora: A Review on Background, Technology, Limitations, and Opportunities of Large Vision Models". In: *CoRR* abs/2402.17177 (2024).
- [8] Ang Wang et al. "Wan: Open and Advanced Large-Scale Video Generative Models". In: *CoRR* abs/2503.20314 (2025).
- [9] Weijie Kong et al. "HunyuanVideo: A Systematic Framework For Large Video Generative Models". In: *CoRR* abs/2412.03603 (2024).
- [10] Fan Bao et al. "Vidu: a Highly Consistent, Dynamic and Skilled Text-to-Video Generator with Diffusion Models". In: *CoRR* abs/2405.04233 (2024).
- [11] Aaron Jaech et al. "OpenAI o1 System Card". In: *CoRR* abs/2412.16720 (2024).
- [12] Tianxing Chen et al. "RoboTwin 2.0: A Scalable Data Generator and Benchmark with Strong Domain Randomization for Robust Bimanual Robotic Manipulation". In: *CoRR* abs/2506.18088 (2025).
- [13] Yucheng Hu et al. "Video Prediction Policy: A Generalist Robot Policy with Predictive Visual Representations". In: *CoRR* abs/2412.14803 (2024).
- [14] Yilun Du et al. "Learning Universal Policies via Text-Guided Video Generation". In: *Advances in Neural Information Processing Systems 36: Annual Conference on Neural Information Processing Systems 2023, NeurIPS 2023, New Orleans, LA, USA, December 10 - 16, 2023*. Ed. by Alice Oh et al. 2023.
- [15] Zipeng Fu, Tony Z. Zhao, and Chelsea Finn. "Mobile ALOHA: Learning Bimanual Mobile Manipulation with Low-Cost Whole-Body Teleoperation". In: *CoRR* abs/2401.02117 (2024).
- [16] Yaron Lipman et al. "Flow Matching for Generative Modeling". In: *The Eleventh International Conference on Learning Representations, ICLR 2023, Kigali, Rwanda, May 1-5, 2023*. OpenReview.net, 2023.
- [17] Xingchao Liu, Chengyue Gong, and Qiang Liu. "Flow Straight and Fast: Learning to Generate and Transfer Data with Rectified Flow". In: *The Eleventh International Conference on Learning Representations, ICLR 2023, Kigali, Rwanda, May 1-5, 2023*. OpenReview.net, 2023.
- [18] AgiBot-World-Contributors et al. "AgiBot World Colosseo: A Large-scale Manipulation Platform for Scalable and Intelligent Embodied Systems". In: *CoRR* abs/2503.06669 (2025).
- [19] Hengkai Tan et al. "AnyPos: Automated Task-Agnostic Actions for Bimanual Manipulation". In: *CoRR* abs/2507.12768 (2025).
- [20] Chengbo Yuan et al. "RoboEngine: Plug-and-Play Robot Data Augmentation with Semantic Robot Segmentation and Background Generation". In: *CoRR* abs/2503.18738 (2025).
- [21] Kun Wu et al. "RoboMIND: Benchmark on Multi-embodiment Intelligence Normative Data for Robot Manipulation". In: *CoRR* abs/2412.13877 (2024).
- [22] Ryan Hoque et al. "EgoDex: Learning Dexterous Manipulation from Large-Scale Egocentric Video". In: *CoRR* abs/2505.11709 (2025).

[23] Olaf Ronneberger, Philipp Fischer, and Thomas Brox. “U-Net: Convolutional Networks for Biomedical Image Segmentation”. In: *Medical Image Computing and Computer-Assisted Intervention - MICCAI 2015 - 18th International Conference Munich, Germany, October 5 - 9, 2015, Proceedings, Part III*. Ed. by Nassir Navab et al. Vol. 9351. Lecture Notes in Computer Science. Springer, 2015, pp. 234–241.

[24] Huazhi Xu, Xiaoyan Luo, and Wencong Xiao. “Multi-residual unit fusion and Wasserstein distance-based deep transfer learning for mill load recognition”. In: *Signal Image Video Process.* 18.4 (2024), pp. 3187–3196.

[25] Ilya Loshchilov and Frank Hutter. “Decoupled Weight Decay Regularization”. In: *7th International Conference on Learning Representations, ICLR 2019, New Orleans, LA, USA, May 6-9, 2019*. OpenReview.net, 2019.

[26] Aaron Hurst et al. “GPT-4o System Card”. In: *CoRR* abs/2410.21276 (2024).

[27] Alec Radford et al. “Learning Transferable Visual Models From Natural Language Supervision”. In: *Proceedings of the 38th International Conference on Machine Learning, ICML 2021, 18-24 July 2021, Virtual Event*. Ed. by Marina Meila and Tong Zhang. Vol. 139. Proceedings of Machine Learning Research. PMLR, 2021, pp. 8748–8763.

[28] Kevin Black et al. “ $\pi_0$ : A Vision-Language-Action Flow Model for General Robot Control”. In: *CoRR* abs/2410.24164 (2024).

[29] Ziqi Huang et al. “VBench: Comprehensive Benchmark Suite for Video Generative Models”. In: *IEEE/CVF Conference on Computer Vision and Pattern Recognition, CVPR 2024, Seattle, WA, USA, June 16-22, 2024*. IEEE, 2024, pp. 21807–21818.

[30] Anthony Brohan et al. “RT-1: Robotics Transformer for Real-World Control at Scale”. In: *Robotics: Science and Systems XIX, Daegu, Republic of Korea, July 10-14, 2023*. Ed. by Kostas E. Bekris et al. 2023.

[31] Brianna Zitkovich et al. “RT-2: Vision-Language-Action Models Transfer Web Knowledge to Robotic Control”. In: *Conference on Robot Learning, CoRL 2023, 6-9 November 2023, Atlanta, GA, USA*. Ed. by Jie Tan, Marc Toussaint, and Kourosh Darvish. Vol. 229. Proceedings of Machine Learning Research. PMLR, 2023, pp. 2165–2183.

[32] Dibya Ghosh et al. “Octo: An Open-Source Generalist Robot Policy”. In: *Robotics: Science and Systems XX, Delft, The Netherlands, July 15-19, 2024*. Ed. by Dana Kulic et al. 2024.

[33] Siyuan Zhou et al. “RoboDreamer: Learning Compositional World Models for Robot Imagination”. In: *Forty-first International Conference on Machine Learning, ICML 2024, Vienna, Austria, July 21-27, 2024*. OpenReview.net, 2024.

[34] Homanga Bharadhwaj et al. “Gen2Act: Human Video Generation in Novel Scenarios enables Generalizable Robot Manipulation”. In: *CoRR* abs/2409.16283 (2024).

[35] Qingwen Bu et al. “Closed-Loop Visuomotor Control with Generative Expectation for Robotic Manipulation”. In: *Advances in Neural Information Processing Systems 38: Annual Conference on Neural Information Processing Systems 2024, NeurIPS 2024, Vancouver, BC, Canada, December 10 - 15, 2024*. Ed. by Amir Globersons et al. 2024.

[36] Kevin Black et al. “Zero-Shot Robotic Manipulation with Pretrained Image-Editing Diffusion Models”. In: *CoRR* abs/2310.10639 (2023).

[37] Hongtao Wu et al. “Unleashing Large-Scale Video Generative Pre-training for Visual Robot Manipulation”. In: *The Twelfth International Conference on Learning Representations, ICLR 2024, Vienna, Austria, May 7-11, 2024*. OpenReview.net, 2024.

[38] Jack Parker-Holder et al. “Genie 2: A Large-Scale Foundation World Model”. In: (2024).

[39] Jiahao Li et al. “Instant3D: Fast Text-to-3D with Sparse-view Generation and Large Reconstruction Model”. In: *The Twelfth International Conference on Learning Representations, ICLR 2024, Vienna, Austria, May 7-11, 2024*. OpenReview.net, 2024.

[40] Shuang Li et al. “Unified Video Action Model”. In: *CoRR* abs/2503.00200 (2025).

[41] Youpeng Wen et al. “VidMan: Exploiting Implicit Dynamics from Video Diffusion Model for Effective Robot Manipulation”. In: *Advances in Neural Information Processing Systems 38: Annual Conference on Neural Information Processing Systems 2024, NeurIPS 2024, Vancouver, BC, Canada, December 10 - 15, 2024*. Ed. by Amir Globersons et al. 2024.

[42] Junbang Liang et al. “Dreamitate: Real-World Visuomotor Policy Learning via Video Generation”. In: *Conference on Robot Learning, 6-9 November 2024, Munich, Germany*. Ed. by Pulkit Agrawal, Oliver Kroemer, and Wolfram Burgard. Vol. 270. Proceedings of Machine Learning Research. PMLR, 2024, pp. 3943–3960.

Table 5: Detailed information about datasets. Dataset instructions correspond to the robot and camera components of the unified observation space (see Figure 1).

Dataset	Dataset Instruction
Agibot	The whole scene is in a realistic, industrial art style with three views: <b>a fixed high camera, a movable left arm camera, and a movable right arm camera</b> . The <b>genie-1 robot</b> is currently performing the following task:
RDT	The whole scene is in a realistic, industrial art style with three views: <b>a fixed front camera, a movable left arm camera, and a movable right arm camera</b> . The <b>aloha robot</b> is currently performing the following task:
RoboMind Franka	The whole scene is in a realistic, industrial art style with three views: <b>a fixed camera on the opposite side, a fixed left camera, and a fixed right camera</b> . The <b>franka robot</b> is currently performing the following task:
RoboMind Aloha	The whole scene is in a realistic, industrial art style with three views: <b>a fixed front camera, a movable left arm camera, and a movable right arm camera</b> . The <b>aloha robot</b> is currently performing the following task:
Egodex	The whole scene is in a realistic, industrial art style with one view: <b>a movable front camera</b> . The <b>person</b> is currently performing the following task:
RoboTwin	The whole scene is in a realistic, industrial art style with three views: <b>a fixed rear camera, a movable left arm camera, and a movable right arm camera</b> . The <b>aloha robot</b> is currently performing the following task:
Vidar	The whole scene is in a realistic, industrial art style with three views: <b>a fixed rear camera, a movable left arm camera, and a movable right arm camera</b> . The <b>aloha robot</b> is currently performing the following task:

## A Dataset Details

The details of our datasets are presented in Table 5. For the RoboTwin dataset, we adjust the camera positions to capture both arms in full, rather than only the end-effectors, to improve training of the masked inverse dynamics model. For the Agibot-World dataset, episodes are segmented into shorter clips using their frame-level annotations. We also filter out episodes with fewer than three views or shorter than four seconds. For each dataset, we provide information about the associated robot and camera setups, which form part of the unified observation space. During pre-training, sampling ratios for each dataset are set proportionally to their sizes. It is worth noting that the RoboTwin dataset and our Vidar dataset differ from all pre-training datasets in these aspects, and we additionally leverage GPT-4o to augment its task annotations.

## B Training and Inference Details

Using 64 NVIDIA Ampere-series 80GB GPUs, we train Vidu 2.0 for 23,000 iterations (10,000 for pre-training and the remainder for fine-tuning), which takes about 64 hours. Note that for all fine-tuning procedures, we employ full-parameter fine-tuning. For MIDM, we use 8 NVIDIA Hopper-series 80GB GPUs for 60,000 training iterations, taking about 5 hours. Additional MIDM hyperparameters are provided in Table 6.

During inference, the video diffusion models are deployed in the cloud, while only the lightweight MIDM is executed locally. For test-time scaling, we uniformly sample 5 – 7 frames from the generated videos and use GPT-4o to select the best result. The prompt we use is shown in Figure 4, focusing on physical plausibility and alignment with the textual instruction.

You are a skilled robot video ranker. Your task is to identify the index of the video with the highest quality based on the provided image clips and video caption. When evaluating the images, consider both their physical accuracy and how well they align with the video caption. Each image contains three views, and you must assess their consistency, ensuring there are no abrupt appearances or disappearances of objects or color blocks between frames. When determining the index, if there is a tie, output the smallest video index. For example: if video 1 has the highest quality, output 1; if video 2 has the highest quality, output 2; if all the videos have the same quality, output 1. We have  $\{n\_videos\}$  videos, each containing  $\{n\_imgs\_per\_video\}$  images, for you to evaluate. The caption for video\_reference is '{caption}'. The images are arranged in the following sequence:

{img\_seq}

Please assess the quality of the videos and provide the index of the one with the highest quality, without any explanations.

Figure 4: Prompt for GPT-4o evaluation. Variables in the curly braces should be replaced by corresponding values. Specifically, one line of “img\_seq” describes one video, and is formatted as “\*\*video\_1\*\*: image\_1, image\_2, ..., image\_{n\_imgs\_per\_video}”.

Table 6: Hyperparameters of MIDM.

Hyperparameter	Value
Number of Parameters	92 Million
U-Net Down-sampling/Up-sampling Layers	5
ResNet Structure	ResNet-50
Action Prediction Loss	Huber Loss
Learning Rate	$5 \times 10^{-4}$
Warm-up	6000 Steps
AdamW $\beta$	(0.9, 0.999)
AdamW $\epsilon$	$10^{-8}$
AdamW Weight Decay	$10^{-2}$

## C Additional Experimental Results

For the simulation experiments, we set  $K = 1$  (i.e., no test-time scaling) for better reproducibility. During testing, we limit the maximum steps to 180, which means there are three model inferences with 60 steps each. The testing success rates averaged over 20 episodes are shown in Table 7.

For the real-world experiments, a more detailed version of Table 1 is provided in Table 8. We also investigate the impact of the hyperparameter  $\lambda$  in MIDM, with results summarized in Table 9 and illustrated in Figure 5. Notably,  $\lambda = 3 \times 10^{-3}$  yields the best performance.

We also test the performance of an existing segmentation model, RoboEngine [20]. As is shown in Figure 6, it often identifies only one arm per frame, fails to recognize grippers in wrist camera views, or lacks temporal consistency across frames.

## D Additional Visualizations of Vidar

More demonstrations, including two failed cases, are shown in Figure 7.

## E Reproduction using the HunyuanVideo Model

We also reproduced our results using the open-source HunyuanVideo Model. The training hyperparameters are detailed in Table 10. Utilizing 64 NVIDIA Hopper-series 80GB GPUs, we trained the model for 12,000 iterations (10,000 for pre-training and the remainder for fine-tuning), which required approximately 54 hours.

Table 7: Success rates of Vidar on the RoboTwin 2.0 benchmark, averaged over 20 episodes. Vidar is trained under the clean scenario with 20 episodes for each task.

Task	Clean	Randomized
Adjust Bottle	100.0%	65.0%
Beat Block Hammer	85.0%	10.0%
Blocks Ranking RGB	55.0%	0.0%
Blocks Ranking Size	35.0%	0.0%
Click Alarmclock	100.0%	35.0%
Click Bell	95.0%	25.0%
Dump Bin Bigbin	50.0%	10.0%
Grab Roller	100.0%	30.0%
Handover Block	5.0%	0.0%
Handover Mic	0.0%	0.0%
Hanging Mug	0.0%	0.0%
Lift Pot	90.0%	10.0%
Move Can Pot	60.0%	0.0%
Move Pillbottle Pad	70.0%	20.0%
Move Playingcard Away	100.0%	40.0%
Move Stapler Pad	35.0%	0.0%
Open Laptop	50.0%	30.0%
Open Microwave	20.0%	0.0%
Pick Diverse Bottles	55.0%	0.0%
Pick Dual Bottles	85.0%	15.0%
Place A2B Left	45.0%	10.0%
Place A2B Right	55.0%	15.0%
Place Bread Basket	75.0%	15.0%
Place Bread Skillet	85.0%	10.0%
Place Burger Fries	80.0%	5.0%
Place Can Basket	50.0%	0.0%
Place Cans Plasticbox	0.0%	0.0%
Place Container Plate	100.0%	55.0%
Place Dual Shoes	0.0%	0.0%
Place Empty Cup	100.0%	20.0%
Place Fan	45.0%	0.0%
Place Mouse Pad	60.0%	10.0%
Place Object Basket	35.0%	10.0%
Place Object Scale	85.0%	0.0%
Place Object Stand	95.0%	35.0%
Place Phone Stand	75.0%	25.0%
Place Shoe	80.0%	40.0%
Press Stapler	90.0%	40.0%
Put Bottles Dustbin	0.0%	0.0%
Put Object Cabinet	0.0%	0.0%
Rotate QRcode	65.0%	10.0%
Scan Object	45.0%	5.0%
Shake Bottle	100.0%	65.0%
Shake Bottle Horizontally	100.0%	60.0%
Stack Blocks Three	15.0%	0.0%
Stack Blocks Two	80.0%	5.0%
Stack Bowls Three	45.0%	15.0%
Stack Bowls Two	95.0%	35.0%
Stamp Seal	50.0%	0.0%
Turn Switch	60.0%	10.0%
Average	60.0%	15.7%

Table 8: Detailed success rates of various methods and configurations on robot manipulation tasks. “L”, “R”, and “B” indicate the use of the left arm, right arm, or both arms, respectively. “w/o TTS” and “w/o MIDM” correspond to the ablation settings described in Table 4.

Scenario/Task	Success Rate				
	UniPi	VPP	<b>Vidar</b>	w/o TTS	w/o MIDM
Seen Tasks & Backgrounds					
Grasp the Tomato (L)	60.0%	0.0%	60.0%	60.0%	80.0%
Grasp the Tomato (R)	20.0%	0.0%	80.0%	60.0%	60.0%
Lift the Basket (B)	66.7%	0.0%	66.7%	33.3%	33.3%
Flip the Dice to Point One on the Top (L)	0.0%	33.3%	33.3%	0.0%	33.3%
Grab the Bottle (L)	0.0%	0.0%	66.7%	33.3%	33.3%
Get the Toast from the Toaster (L)	66.7%	0.0%	100.0%	66.7%	100.0%
Average	36.4%	4.5%	<b>68.2%</b>	45.5%	59.1%
Unseen Tasks	UniPi	VPP	<b>Vidar</b>	w/o TTS	w/o MIDM
Place the Bowl on the Steamer (L)	0.0%	0.0%	66.7%	66.7%	33.3%
Grasp the Shortest Bread (L)	0.0%	0.0%	66.7%	33.3%	0.0%
Grasp the Shortest Bread (R)	0.0%	0.0%	66.7%	33.3%	33.3%
Wipe the Table with Rag (L)	33.3%	33.3%	66.7%	33.3%	66.7%
Wipe the Table with Rag (R)	0.0%	33.3%	66.7%	0.0%	0.0%
Average	6.7%	13.3%	<b>66.7%</b>	33.3%	26.7%
Unseen Backgrounds	UniPi	VPP	<b>Vidar</b>	w/o TTS	w/o MIDM
Grasp the Tomato (L)	0.0%	0.0%	66.7%	33.3%	0.0%
Flip the Die to Point One on the Top (L)	0.0%	0.0%	33.3%	33.3%	0.0%
Flip the Die to Point One on the Top (R)	0.0%	0.0%	33.3%	0.0%	0.0%
Pick the Carrot on the Green Plate (L)	33.3%	0.0%	33.3%	66.7%	0.0%
Place the Bowl on the Plate (L)	33.3%	0.0%	66.7%	66.7%	33.3%
Place the Bowl on the Plate (R)	66.7%	0.0%	100.0%	66.7%	100.0%
Average	22.2%	0.0%	<b>55.6%</b>	44.4%	22.2%

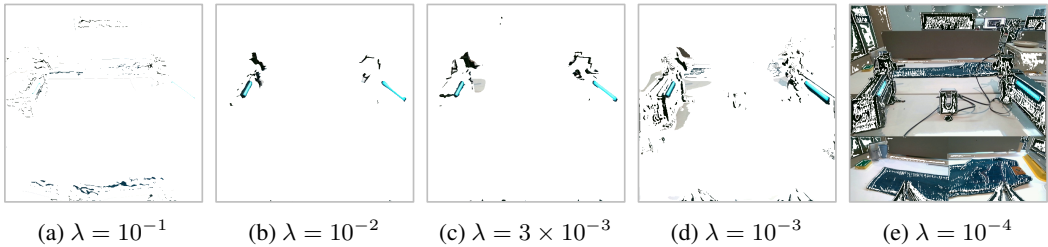


Figure 5: Masked images learned by the masked inverse dynamic model (MIDM) with different values of  $\lambda$ .



Figure 6: Segmentation results. We split the concatenated video frames into three views and apply RoboEngine [20] to each view.

Table 9: Analysis of hyperparameter  $\lambda$  in the masked inverse dynamics model. The success rates are robust over a large range, and  $\lambda = 3 \times 10^{-3}$  achieves the best performance.

$\lambda$	Training Accuracy	Testing Accuracy	Testing $l_1$ Error
$10^{-1}$	99.1%	7.1%	0.0670
$10^{-2}$	99.8%	39.9%	0.0331
$3 \times 10^{-3}$	<b>99.9%</b>	<b>49.0%</b>	<b>0.0308</b>
$10^{-3}$	99.9%	40.7%	0.0338
$10^{-4}$	99.8%	24.4%	0.0461

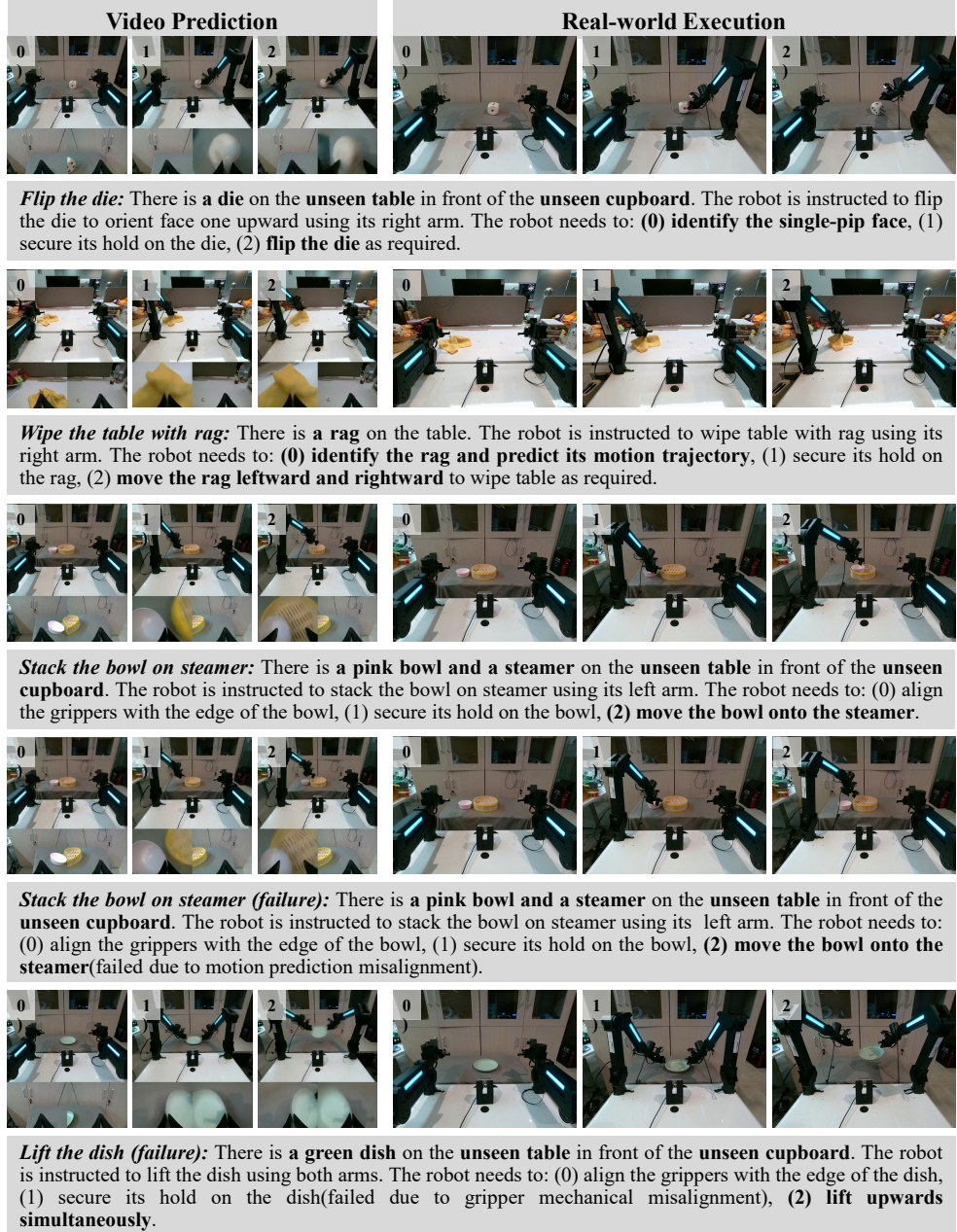


Figure 7: Videos of predictions (left) and corresponding executions (right) of Vidar for more challenging tasks. Both successful and failed cases are presented.

Table 10: Hyperparameters of the HunyuanVideo Model.

Hyperparameter	Value
Number of Parameters	13 Billion
Learning Rate (Pre-train)	$1 \times 10^{-4}$
Learning Rate (Fine-tune)	$5 \times 10^{-5}$
Warm-up	500 Steps
Optimizer	AdamW
AdamW $\beta$	(0.9, 0.999)
AdamW $\epsilon$	$10^{-8}$
AdamW Weight Decay	0

Table 11: Success rates of Vidar reproduced using the HunyuanVideo Model.

Task	Success Rate
Grasp the Apple (Seen Task)	75.0%
Grab the Bottle (Seen Task)	100.0%
Grasp the Cup by its Handle (Seen Task)	25.0%
Lift the Steamer (Unseen Task)	50.0%
Grasp the Apple and Put it into the Steamer (Unseen Task)	100.0%
Stack One Cube on Top of the Other Cube (Unseen Task)	20.0%
Average	58.3%

Due to limited resources, we evaluated the model on six tasks. The results are presented in Table 11 and Figure 8. We plan to open-source our implementations related to both the HunyuanVideo Model and our MIDM.

## F Hardware Details

Hardware details are shown in Figure 9 and Table 12. One important assumption underlying this approach is that the intermediate video modality contains all the information for action prediction. However, this assumption fails to hold for many robotic systems due to the specific platform setting, including the Aloha platform. In the pre-training part of Figure 1, we can see that the arm joints frequently fall outside the camera’s field of view, even with three different views available. In our target domain, we adjust the center camera to a new position where two arms can be fully captured, shown in the fine-tuning part of Figure 1. In this way, our robotic platform differs from any platform we encountered during pre-training, serving as an ideal testbed for showing adaptation capability with scarce data.

## G Large Language Model Usage

We utilize large language models to refine the writing. For example, we write a draft and let the model check the grammar errors.

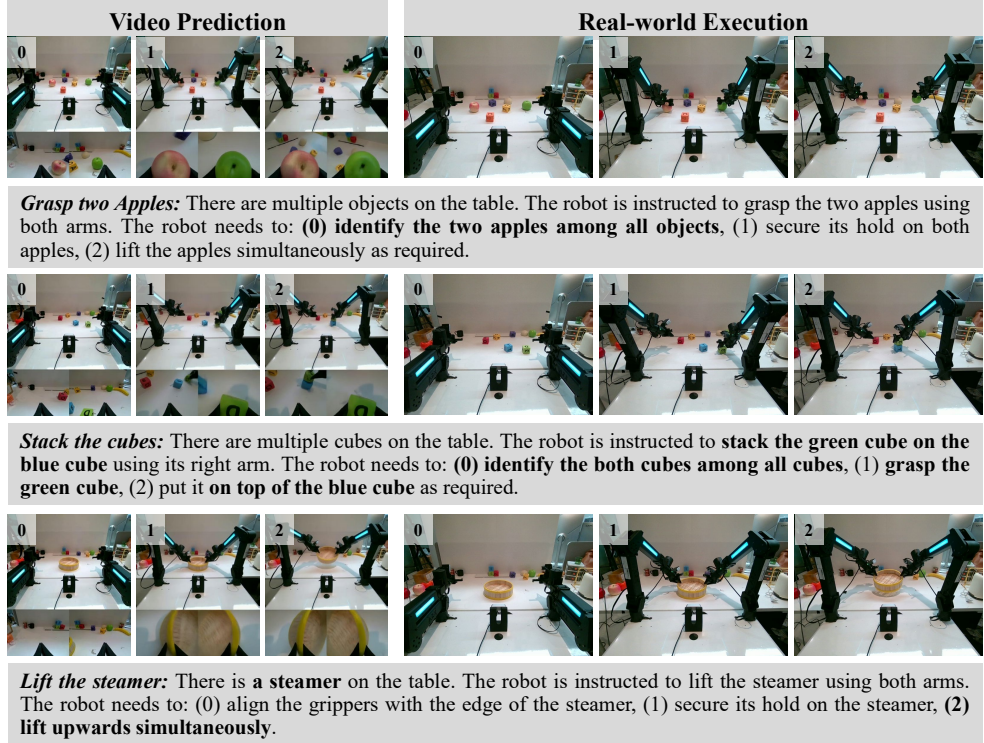


Figure 8: Videos of predictions (left) and corresponding executions (right) of Vidar reproduced using the HunyuanVideo model for challenging tasks.



Figure 9: Our robotic platform.

Table 12: Hardware Information.

Parameter	Value
Degree of Freedom	$2 \times (6 + 1) = 14$
Cameras	3 RGB Cameras
Arm weight	3.9 kg
Arm Valid Payload	1.0 kg
Arm Reach	0.6 m
Arm Repeatability	1 mm
Gripper Range	0 - 80 mm
Gripper Max Force	10 N